



CHORUS

This is the accepted manuscript made available via CHORUS. The article has been published as:

Solubility and clustering of ruthenium fission products in uranium dioxide as determined by density functional theory

Minki Hong (□□□), Simon R. Phillpot, Chan-Woo Lee, Pankaj Nerikar, Blas P. Uberuaga, Christopher R. Stanek, and Susan B. Sinnott

Phys. Rev. B **85**, 144110 — Published 16 April 2012

DOI: [10.1103/PhysRevB.85.144110](https://doi.org/10.1103/PhysRevB.85.144110)

Solubility and Clustering of Ruthenium Fission Products in Uranium Dioxide as Determined by Density Functional Theory

Minki Hong(홍민기)¹, Simon R. Phillpot¹, Chan-Woo Lee^{1,+}, Pankaj Nerikar², Blas P. Uberuaga²,
Christopher R. Stanek², and Susan B. Sinnott^{1,*}

¹Department of Materials Science and Engineering, University of Florida, Gainesville, FL 32611

²Materials Science and Technology Division, Los Alamos National Laboratory, Los Alamos, NM 87545

Abstract

One of the consequences of the fission process in UO₂ fuels in nuclear reactors is the eventual formation of metallic fission product inclusions and precipitates. Here the stability and clustering behavior of one particular metallic fission product – Ru – is investigated using density functional theory in combination with classical thermodynamics. In particular, the solution energies of individual Ru atoms, dimers, and trimers at interstitial, uranium and oxygen vacancy, divacancy, and Schottky defect sites are calculated. Ru is predicted to be insoluble in most cases, but is soluble in uranium vacancy sites under hyper-stoichiometric conditions (UO_{2+x}). Density of states analysis reveals the metallic nature of even the smallest Ru aggregates. Finally, by analyzing the binding characteristics of Ru in UO₂, metallic dimers in Schottky defects are identified as the probable nucleus of metallic precipitates in UO₂.

* Corresponding author, email: ssinn@mse.ufl.edu

⁺ Current address: The Makineni Theoretical Laboratories, Department of Chemistry, University of Pennsylvania, Philadelphia, PA 19104

1. Introduction

The chemical stability of fission products (FPs) in uranium dioxide (UO₂) based nuclear fuels is critical to both the performance and the integrity of the fuel. There is, therefore, tremendous interest in understanding the microscopic behavior of FPs under the operating conditions of the fuel, including high temperature and irradiation. For decades, atomic scale calculation and simulation methods have been used to quantify this chemical stability¹⁻³. A typical starting point is the calculation of the solution energy of fission products as point defects in the UO₂ matrix³. Among the various computational approaches that can be used to calculate these energies, density functional theory (DFT) is one of the most widely employed today because of its ability to produce relatively high-fidelity results for both a wide range of fission products and for UO₂, as well as to account for the complexities associated with different bonding environments within one system. However, the conditions of typical DFT calculations (zero Kelvin and perfect vacuum) are inconsistent with the conditions in actual reactors (high temperatures and oxygen partial pressures). An approach that addresses this limitation while retaining the strengths of the DFT approach is to combine the results of DFT calculations with thermodynamics calculations⁴⁻⁷.

In the past, DFT calculations have most commonly been applied to examine the accommodation of fission products as point defects, which is most relevant to the very earliest stages of fission product formation and accommodation. An improved description of fission product formation and incorporation over longer times, however, requires consideration of more complicated defect structures, such as fission product clusters, bubbles, inclusions, and precipitates. These types of extended defects have been most commonly examined using less computationally intensive empirical methods, than DFT, which limits the types of aggregates that can be studied^{8, 9}. Recently, however, enhanced by the capabilities of

modern computing systems, it is possible to apply DFT to examine small-scale defect clusters in UO_2 that may form the nuclei of larger fission product aggregates.

The solution energy of Kr, a gaseous fission product which has high yield, was among the first to be considered in DFT calculations¹⁰. The resulting energies at several intrinsic defects predicted that Kr is insoluble in UO_2 , in agreement with experimental findings¹¹ and pair potential calculations^{3, 12}. This insolubility was also predicted by a subsequent computational study¹³ which presented the dependence of the solubility of fission products on the thermodynamic conditions of the fuel such as stoichiometry, defect concentration, and temperature. In addition, over the last decade, the chemical stability of various fission products that exist in gaseous or oxide form in UO_2 – including He, I, Cs, Sr, Ba, Zr, Mo, and Xe – have been determined using DFT¹³⁻¹⁷. More recently, the stabilities of selected metallic fission products were also examined¹⁸. In most cases these studies focused on a single fission product atom and its solution or oxide formation at trap sites, the stabilities of which were also evaluated using DFT¹⁹⁻²³. Because these studies focused on individual FPs within the UO_2 host, the FP was typically in an oxidized state, and not representative of metallic precipitation.

Here, the focus is on the solubility of metallic Ru fission products, examined using a combination of DFT and classical thermodynamics in a manner similar to that taken in Refs^{5, 6, 24, 25}. Ruthenium can typically be found in the form of metallic (or “white”) inclusions within the fuel, normally an alloy of metallic FPs: Ru, Mo, Pd, Rh, Tc and Te¹¹. There is little information, however, about the atomic scale accommodation of these metallic fission products and their influence on fuel performance. We first consider the chemical stability of various Ru complexes of different sizes to quantify how the very initial stages of metallic fission product clustering influences solution energies and the electronic structure of the fuel.

2. Computational Details

2.1 Electronic Structure Calculations

The DFT calculations for total energies are carried out with the projector-augmented-wave method (PAW)²⁶ as implemented in the Vienna Ab Initio Simulation Package (VASP)^{27, 28}. The valence electrons considered are as follows: U $6s^2 6p^6 5f^3 6d^1 7s^2$, O $2s^2 2p^4$, and Ru $4s^1 3d^7$. The outermost core radii are 2.80, 1.52, and 2.60 in a.u. for U, O, and Ru, respectively. Slight overlaps are found only for Ru-O bonds in Ru cluster systems, as discussed in Section 3.2. These overlaps are less than those that occur in ruthenium oxides using the same core radii and for which PAW calculations provide good agreement with experiment^{29, 30}. Thus the effect of overlap is expected to be negligible. While in most cases the local density approximation (LDA) and generalized gradient approximation (GGA)³¹ to the exchange and correlation energies within DFT provide reasonably accurate descriptions of the electronic structure of most materials, it is now established that these approximations have difficulties in describing the ground-state behavior of highly correlated materials, including actinide oxides³². The suggested reason for this shortcoming is the partial filling of the $5f$ orbitals and the resulting strong correlation, which means that electrons tend to be localized rather than dispersed over the entire system³³. As a result, DFT calculations using the LDA or GGA, which delocalize electrons too strongly, incorrectly predict that insulating UO_2 is metallic. Several attempts have been made to address this shortcoming including the Hubbard+ U approach³⁴⁻³⁶, self-interaction correction (SIC)³⁷, and hybrid functionals for exchange and correlation³⁸. Here, we utilize the GGA+ U framework to capture the strong correlated nature of the $5f$ electrons of uranium. The $U_{\text{eff}}(\text{U-J})$ value is chosen as 3.96 eV, as was the case in other studies^{17, 19, 22, 39}. Recently, metastable states of pure UO_2 have been explored by modifying occupation matrices^{40, 41}. However, it has been established that the degeneracy associated

with metastable states is broken in systems with low symmetry, such as the defect configurations studied here. Therefore metastable states are unlikely and their exploration is left for future work.

To model the bulk UO_2 system we use a $2 \times 2 \times 2$ supercell with 96 atoms for the structural optimizations, and the cell volume is kept constant during the determination of Ru atomic, dimer, and trimer solution energies in order to better mimic their incorporation within an actual extended UO_2 lattice. This is admittedly a small supercell and thus it is necessary to check that our results are converged against Brillouin zone sampling. For all of the calculations reported here we sampled the Brillouin zone with a $2 \times 2 \times 2$ Monkhorst–Pack k -point mesh⁴². We considered the effect of k -mesh density on the defect formation energy in UO_2 in a manner that is similar to a previous study⁴³; the results are given in Table 1. We also implemented a similar k -mesh test for the Ru- UO_2 system that is discussed in the next section and confirmed that the difference in solution energy between $2 \times 2 \times 2$ and $4 \times 4 \times 4$ sampling is in the range of sub-meV. This indicates that a $2 \times 2 \times 2$ mesh is sufficient to avoid significant numerical errors in the calculations. The cutoff energy for the plane-waves is 400 eV for all the calculations reported here. The convergence criteria for the energy difference was 10^{-5} eV and for the residual forces less than 10^{-2} eV/Å.

Table 1. Defect formation energy of uranium vacancy in UO_2 for different k -meshes

| k -mesh | Defect formation energy of V_U (eV) |
|-----------------------|---------------------------------------|
| $1 \times 1 \times 1$ | 8.598 |
| $2 \times 2 \times 2$ | 9.675 |
| $4 \times 4 \times 4$ | 9.761 |

2.2 Thermodynamic Calculations

The solution energy E_{solution} of a fission product is defined as³

$$E_{\text{solution}} = E_{\text{inc}} + E_{\text{trap}}, \quad (1)$$

where E_{inc} is the incorporation energy of a given fission product at a pre-existed trap site, and E_{trap} is the trap site formation energy, the energy required to form the trap site for the incorporation of the fission product. Detailed definitions of these energies are discussed elsewhere¹⁷. We can calculate the incorporation energy using total energies from DFT calculations as:

$$E_{inc} = E^{total}(i) - E^{total}(\text{trap site}) - E_i. \quad (2)$$

$E^{total}(i)$ is the total energy of the system with a fission product i at a specific trap site, $E^{total}(\text{trap site})$ is the total energy of the system with the trap site only, and E_i is the total energy of a single atom i , i.e., the chemical potential of i ; this is discussed in detail in section 2.3. Because the incorporation energy applies to a situation where the trap sites already exist in the fuel and that they greatly outnumber the fission products generated, the actual fuel condition after a certain amount of burn up is not accounted for properly. In other words, the concentration of a given trap site within the fuel, which is a function of a variety of experimental factors including burn-up, temperature, and stoichiometry of the fuel, can then be used to calculate the solution energy for arbitrary conditions. Therefore, the energy needed to form trap sites is determined by combining the results of DFT with classical thermodynamics calculations. A common approach for considering thermodynamics is to utilize the point defect model (PDM)^{24, 44} to evaluate the effect of fuel stoichiometry and temperature on the trap site formation energy, which can be expressed as:

$$E_{trap} = -kT \ln([X]). \quad (3)$$

Here $[X]$ is the concentration of the defect considered and is found by solving self-consistently the coupled reactions for all of the relevant defects in the material. Analytical expressions for E_{trap} for various trap sites within the low temperature limit where only one trap site dominates the incorporation of a given fission product can be derived and are tabulated in Table 2^{1, 16}. They can be seen to depend on

the deviation of the fuel from stoichiometry (x), the formation energies of oxygen Frenkel pairs (E_{FPO}) and Schottky defects (E_{Sch}), and the binding energies of divacancies and trivacancies ($B_{\text{DV}}, B_{\text{Sch}}$)^{3, 14}.

Table 2. Trap site formation energies of defects in UO_2 ^{1, 16}

| Trap Site | Formation energy | | |
|----------------|---|---|---|
| | UO_{2-x} | UO_2 | UO_{2+x} |
| V_{O} | $-kT \ln\left(\frac{ x }{2}\right)$ | $\frac{E_{\text{FPO}}}{2} + \frac{kT}{2} \ln(2)$ | $E_{\text{FPO}} + kT \ln(x)$ |
| V_{U} | $2kT \ln\left(\frac{ x }{2}\right) + E_{\text{Sch}}$ | $E_{\text{Sch}} - E_{\text{FPO}} - kT \ln(2)$ | $E_{\text{Sch}} - 2E_{\text{FPO}} - 2kT \ln(x)$ |
| DV | $E_{\text{Sch}} - B_{\text{DV}} + kT \ln\left(\frac{ x }{2}\right)$ | $E_{\text{Sch}} - \frac{E_{\text{FPO}}}{2} - B_{\text{DV}} - \frac{kT}{2} \ln(2)$ | $E_{\text{Sch}} - E_{\text{FPO}} - B_{\text{DV}} - kT \ln(x)$ |
| Sch | $E_{\text{Sch}} - B_{\text{Sch}}$ | $E_{\text{Sch}} - B_{\text{Sch}}$ | $E_{\text{Sch}} - B_{\text{Sch}}$ |

2.3 Allowed Chemical Potential

To calculate the energies discussed in the last section, the energy of a single atom must be defined. One of the most commonly used ways of doing this is to take an isolated atom which is infinitely far from the system as a reference. Under those conditions, the total energy of a single atom is calculated by the self-interaction energy of DFT. An alternative approach is to use the atom in its standard state as the reference instead of the isolated atom. In this case, the total energy of a single atom is defined as the energy per atom in each of the reference systems. These different approaches essentially define different chemical potentials for the relevant species. For UO_2 , we use the later approach, taking the reference state of oxygen as an oxygen molecule (O_2) in the gas phase and the reference state of uranium as bulk metal ($\alpha\text{-U}$). For the fission product (Ru), both approaches are considered to determine the single atom energy (see details in section 3). The GGA+ U approach is used because of its ability to reproduce the electronic structure of UO_2 . However, while GGA+ U does not

accurately describe the structure of α -U (see Table 3) due to the weak electron correlations present in the metal⁴⁵, we nevertheless apply the $+U$ scheme to α -U in order to maintain consistency with the calculations for the UO_2 system; this constraint does not alter the energetic trends. We note that $+U$ still predicts α -U to be metallic.

Table 3. Lattice parameters of α -U

| Lattice parameter(Å) | GGA | GGA+U | Exp. ⁴⁶ |
|----------------------|-------|-------|--------------------|
| a | 2.739 | 3.338 | 2.836 |
| b | 5.852 | 5.956 | 5.866 |
| c | 4.965 | 5.715 | 4.935 |

The total internal energy at zero temperature calculated in DFT does not include zero-point vibrations. Therefore, the chemical potential of an atom can be written as

$$\mu(T, P) = E^{total} + \Delta\mu(T, P), \quad (4)$$

where E^{total} is the total energy of the atom and $\Delta\mu(T, P)$ includes the zero-point vibrational energy and the temperature and pressure dependence of the chemical potential^{20, 47}. This term can be simplified by neglecting the zero-point vibrations and the pressure effects. These are reasonable approximations, particularly for defect energy calculations at zero temperature^{6, 47}. The resulting chemical potential of an atom is thus its energy as calculated by DFT according to:

$$\mu(T=0) \approx E^{total}. \quad (5)$$

Thus the chemical potentials of uranium and oxygen are related by the Gibbs free energy of UO_2 bulk:

$$\mu_{\text{U}[\text{UO}_2]} + 2\mu_{\text{O}[\text{UO}_2]} = g_{\text{UO}_2}^{bulk} \approx E_{\text{UO}_2}^{total} \quad (6)$$

where g^{bulk} is the Gibbs free energy per formula unit and E^{total} is the total energy. Eq. (6) applies at equilibrium thus if one of these chemical potentials becomes very low, the oxide would decompose into α -U and oxygen molecules, which are the reference states used for each element. To maintain the oxide form, therefore, the range of chemical potentials is limited. For example, when α -U starts to form as a

result of decomposition, its chemical potential reaches a maximum, which is the chemical potential at the reference state:

$$\mu_{U[UO_2]}^{\max} = \mu_{U[\alpha-U]} \approx E_{\alpha-U}^{\text{total}}. \quad (7)$$

This is called the ‘‘uranium-rich limit’’ of the system and the calculated $E_{\alpha-U}^{\text{total}}$ using GGA+ U is -8.08 eV.

Together with Eq. (6), the minimum of the oxygen chemical potential in UO_2 can be set as:

$$\mu_{O[UO_2]}^{\min} = \frac{1}{2} [g_{UO_2}^{\text{bulk}} - \mu_{U[UO_2]}^{\max}] = \frac{1}{2} [g_{UO_2}^{\text{bulk}} - \mu_{U[\alpha-U]}] \approx \frac{1}{2} [E_{UO_2}^{\text{total}} - E_{\alpha-U}^{\text{total}}]. \quad (8)$$

Similarly we can obtain the maximum of the oxygen chemical potential, which we denote the ‘‘oxygen-rich limit’’:

$$\mu_{O[UO_2]}^{\max} = \mu_{O[O_2]} \approx \frac{1}{2} E_{O_2}^{\text{total}}, \quad (9)$$

where the calculated $\frac{1}{2} E_{O_2}^{\text{total}}$ is -4.89 eV.

Using these upper and lower bounds of oxygen chemical potential, we can set a range of allowed oxygen chemical potentials as originally suggested by Reuter *et al.* for the RuO_2 system⁶ and applied to UO_2 by Yu *et al.*⁴⁸:

$$\begin{aligned} \mu_{O[UO_2]}^{\min} < \mu_{O[UO_2]} < \mu_{O[UO_2]}^{\max}, \\ \frac{1}{2} [g_{UO_2}^{\text{bulk}} - \mu_{U[\alpha-U]}] < \mu_{O[UO_2]} < \mu_{O[O_2]}, \\ \frac{1}{2} [E_{UO_2}^{\text{total}} - E_{\alpha-U}^{\text{total}}] \lesssim \mu_{O[UO_2]} \lesssim \frac{1}{2} E_{O_2}^{\text{total}}. \end{aligned} \quad (10)$$

Although UO_2 is the dominant phase in the actual fuel, highly oxidized phases such as U_3O_8 and UO_3 begin to form as the burn-up proceeds and an anion-excess condition consequently develops. Thus we can set equilibriums similar to the Eq. (6) for these phases:

$$3\mu_{U[U_3O_8]} + 8\mu_{O[U_3O_8]} = g_{U_3O_8}^{\text{bulk}} \approx E_{U_3O_8}^{\text{total}}, \quad (11)$$

$$\mu_{U[UO_3]} + 3\mu_{O[UO_3]} = g_{UO_3}^{bulk} \approx E_{UO_3}^{total} . \quad (12)$$

By assuming the allowed range in the chemical potential for oxygen in UO_2 as a global bound over all phases, the uranium chemical potential range, which varies with the phase considered, can be determined as shown in Fig 1. The oxide with lowest uranium chemical potential varies from UO_2 to UO_3 within this oxygen potential range and this may imply the gradual transition to highly oxidized phases as the oxygen chemical potential increases even though these phases are only available near the oxygen-rich limit. This phase variation corresponds well with the experimental phase diagram of UO_2 , which shows a very narrow region of UO_{2-x} while a wide variety of UO_{2+x} is present. Thus, the chemical potential of each atom must be carefully chosen with regard to both environmental conditions and possible phases in order to determine energies related to defects in UO_2 . The defect formation energies of U and O vacancies using different chemical potentials are given in Table 4 to illustrate this point.

Fig 1. The allowed chemical potentials in various uranium oxides

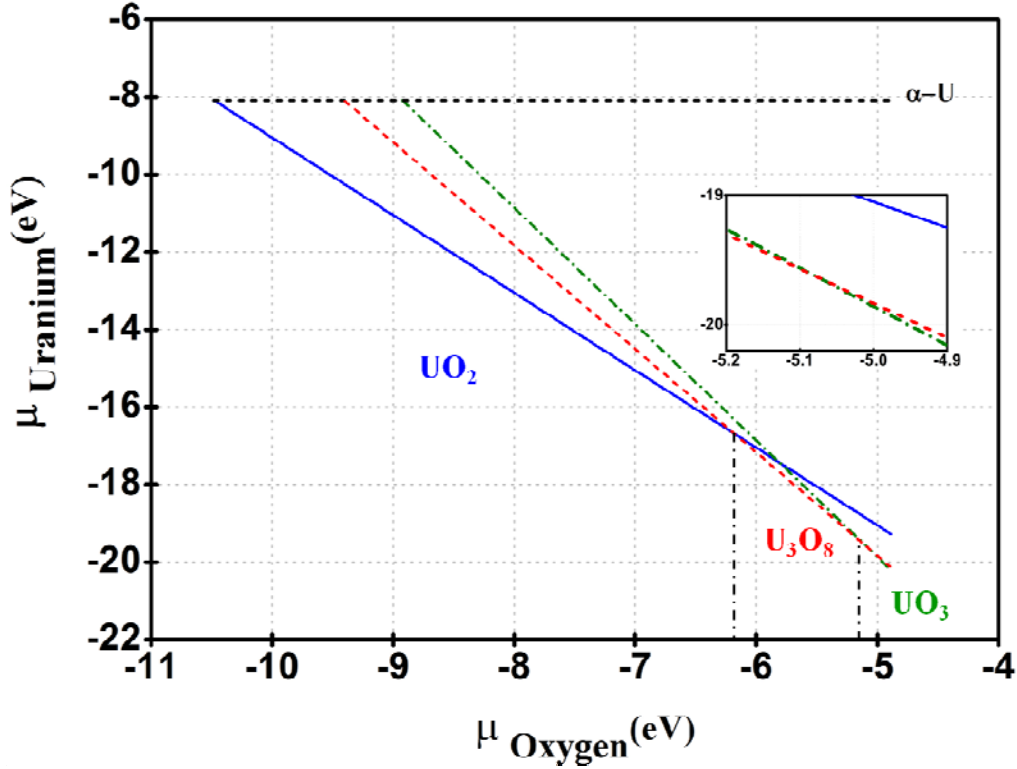


Table 4. Defect formation energies (eV) of uranium and oxygen vacancies; it is assumed that UO_2 phase is maintained under O-rich conditions.

| Defect | U-rich | Intermediate | O-rich |
|-----------------------|--------------------------|---------------------------|---------------------------|
| | | $\mu_{\text{O}} = -10.48$ | $\mu_{\text{O}} = -7.5$ |
| | $\mu_{\text{U}} = -8.08$ | $\mu_{\text{U}} = -14.05$ | $\mu_{\text{U}} = -19.28$ |
| V_{O} | -0.74 | 2.25 | 4.86 |
| V_{U} | 9.67 | 3.71 | -1.52 |

3. Results and Discussion

3.1 Stability of Ru in UO_2

Determining the chemical potential of Ru, μ_{Ru} , is more complicated than determining μ_{U} and μ_{O} . This is because during the fission reaction, Ru is generated as a single atom with high kinetic

energy and is eventually incorporated into UO_2 along with defects produced during the collision or other fission products around it. Therefore we might need to apply different μ_{Ru} depending of the form Ru takes within the matrix (atomic clusters, compounds, oxides, and so on). The easiest approach is to use either gas phase or bulk metal for all case and so we take both references into account for all calculations. The chemical potentials of Ru under different reference states are presented in Table 5.

Table 5. The chemical potentials of Ru (μ_{Ru}) for different reference states

| Reference state | μ_{Ru} | Cohesive energy (eV) |
|-----------------|-------------------|----------------------|
| Isolated atom | -1.39 | - |
| Bulk metal | -9.20 | -7.81 |

For a better assessment of the chemical potential of Ru, however, we may need to consider other possible phases in which Ru can reside in UO_2 rather than Ru metal, such as U-Ru compounds and ruthenium oxides. To enable this, we can expand the allowed chemical potential scheme for UO_2 to these various fission products and thus correlate μ_{Ru} with μ_{U} and μ_{O} . Here, several compounds and oxides are taken into account via their equilibrium equations:

$$2\mu_{\text{U}[\text{U}_2\text{Ru}]} + \mu_{\text{Ru}[\text{U}_2\text{Ru}]} = g_{\text{U}_2\text{Ru}}^{\text{bulk}} \approx E_{\text{U}_2\text{Ru}}^{\text{total}} \quad (13)$$

$$\mu_{\text{U}[\text{URu}_3]} + 3\mu_{\text{Ru}[\text{URu}_3]} = g_{\text{URu}_3}^{\text{bulk}} \approx E_{\text{URu}_3}^{\text{total}} \quad (14)$$

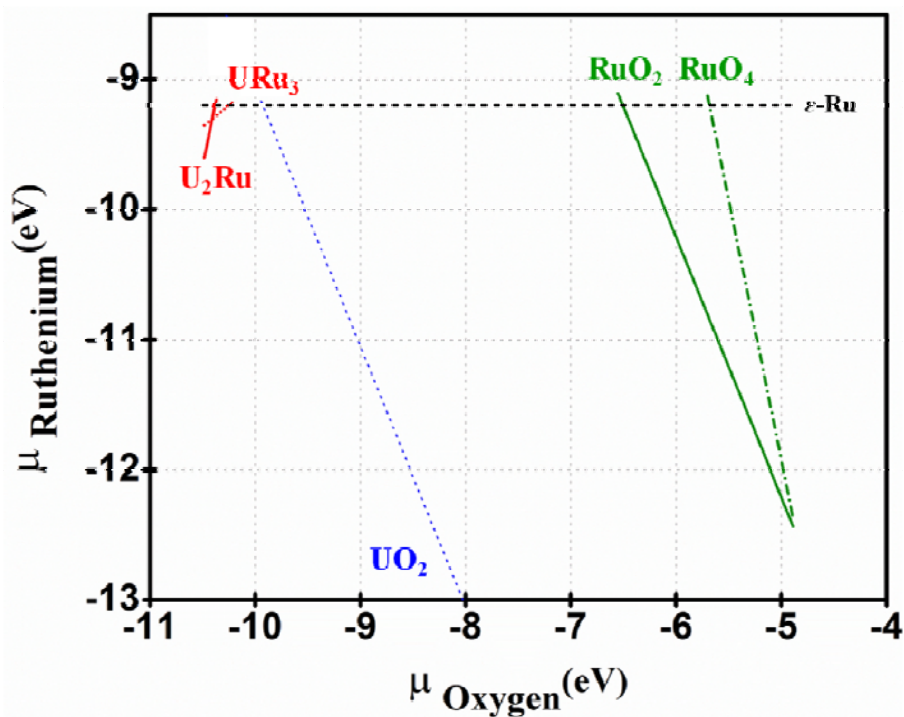
$$\mu_{\text{Ru}[\text{RuO}_2]} + 2\mu_{\text{O}[\text{RuO}_2]} = g_{\text{RuO}_2}^{\text{bulk}} \approx E_{\text{RuO}_2}^{\text{total}} \quad (15)$$

$$\mu_{\text{Ru}[\text{RuO}_4]} + 4\mu_{\text{O}[\text{RuO}_4]} = g_{\text{RuO}_4}^{\text{bulk}} \approx E_{\text{RuO}_4}^{\text{total}} \quad (16)$$

The maximum of μ_{Ru} is the total energy per atom of Ru, which is -9.20 eV (see Table 5). By using this maximum and the equations above, we can obtain the possible chemical potential range of Ru in UO_2 within the allowed range of oxygen discussed in the last section (see Fig 2). Note that μ_{Ru} already

reaches its maximum over a wide range of μ_o and this is consistent with the fact that Ru mostly exists as metallic inclusions in UO_2 . μ_{Ru} can be considerably reduced by forming oxides; however, RuO_x is only stable in UO_2 at very high μ_o as shown in Fig 2 and elsewhere^{18,49}. Therefore, we can reasonably presume that Ru exists in a metallic form rather than a compound or oxide in UO_2 unless the oxygen chemical potential reaches both limits. Hence, it seems reasonable to expect the metal bulk to be the appropriate reference state of Ru in UO_2 , even though the actual Ru may not have the metallic properties. However, for completeness, both reference states are considered for comparison.

Fig 2. The chemical potential of Ru in UO_2 within the allowed oxygen chemical potential



The incorporation energies of Ru at various trap sites are presented in Table 6 using the reference states given in Table 5. Using isolated Ru atom as the reference, the results indicate that Ru incorporates into UO_2 at all trap sites considered. However, as the reference state is adjusted to the bulk metal, the

signs of the incorporation energies become positive. Regardless of the reference state, the U vacancy is the most energetically favorable trap-site for Ru incorporation, as it is for several other fission products^{17, 18}.

Table 6. Incorporation energies of Ru at various trap-sites using different reference states; the lowest energies are denoted in bold.

| Trap site | Incorporation energy (eV) | |
|----------------|----------------------------------|---------------------------|
| | Ref. state: isolated atom | Ref. state: bulk metal |
| Interstitial | -1.11 (-2.46 [*]) | 6.69 |
| V _O | -2.90 (-4.87 [*]) | 4.90 |
| V _U | -7.29 (-7.63[*]) | 0.51 |
| DV | -4.84 (-7.42 [*]) | 2.96 |
| Sch | -5.48 (-5.85 [*]) | 2.33 |

^{*} ref¹⁸

The calculated solution energies of Ru are given in Table 7. Trap-site formation energies are determined using PDM at 0K (as described in Table 2). The stoichiometric deviation is fixed at 0.02 which is within the stoichiometry range where oxygen clustering is negligible, consistent with the assumptions of PDM^{23, 50}. The trend for solution energies with respect to reference states is quite similar to that of incorporation energies. If we choose the isolated atom as the reference, the Ru atoms are soluble in UO_{2+x} for most cases. On the other hand, using the bulk metal as the reference indicates that Ru is insoluble in UO_{2+x} unless the Ru is trapped at a U vacancy in UO_{2+x}. These quantities were also calculated by Brillant *et al.*¹⁸ and Busker *et al.*⁵¹ using DFT and empirical potentials respectively; their results are given in Table 7 for comparison. The calculation criteria Brillant used are different from ours and the empirical potential inherently lacks the capability of calculating single atom energy with proper reference state thus the magnitude of the solution energies from both the DFT and the empirical

potentials is quite different. However, the physical trends are similar to each other (as has been shown to the case for other comparisons of FP solution energy between DFT and pair potentials¹⁷).

Table 7. Solution energies of Ru at various trap-sites using different reference states; the lowest energies are denoted in bold.

| Trap site | Solution energy (eV) | | | | | |
|----------------|------------------------------------|-------------------------------------|------------------------------------|-------------------------------------|---|-------------------------------------|
| | Isolated atom | | | Bulk metal | | |
| | UO _{1.98} | UO ₂ | UO _{2.02} | UO _{1.98} | UO ₂ | UO _{2.02} |
| Interstitial | -1.11 (-2.46 [*]) | -1.11 (-2.46 [*]) | -1.11 (-2.46 [*]) | 6.69 (20.71 ^{**}) | 6.69 (17.26 ^{**}) | 6.69 (13.81 ^{**}) |
| V _O | -2.90 (-4.87 [*]) | -0.41 (-2.87 [*]) | 2.09 (-0.87 [*]) | 4.90 (24.94 ^{**}) | 7.40 (24.90 ^{**}) | 9.90 (24.85 ^{**}) |
| V _U | 0.91 (-0.43 [*]) | -4.08 (-4.43 [*]) | -9.08 (-8.43 [*]) | 8.72 (15.85 ^{**}) | 3.72 (5.59 ^{**}) | -1.27 (-4.66 ^{**}) |
| DV | -1.28 (-4.12 [*]) | -3.78 (-6.12 [*]) | -6.27 (-8.12 [*]) | 6.53 (14.99 ^{**}) | 4.03 (8.14 ^{**}) | 1.53 (1.28 ^{**}) |
| Sch | -2.76 (-4.35 [*]) | -2.76 (-4.35 [*]) | -2.76 (-4.35 [*]) | 5.05 (16.09 ^{**}) | 5.05 (12.64 ^{**}) | 5.05 (9.19 ^{**}) |

^{*} DFT calculations in ref.¹⁸ ^{**} Atomistic calculations in ref.⁵¹

3.2 Clustering Behavior of Ru

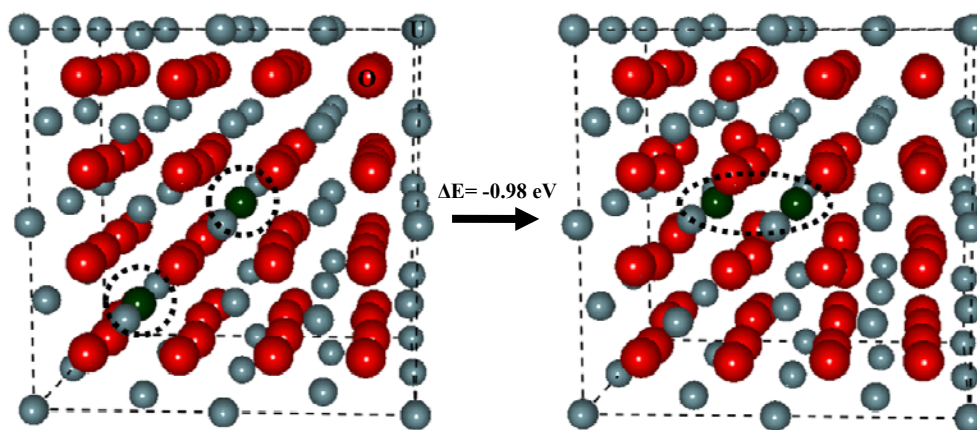
In the previous section, we focused on the solution of individual Ru atoms within UO₂. In the actual fuel, however, Ru tends to form metallic clusters in the UO₂ pellet rather than exist as dispersed atoms¹¹. Therefore understanding the clustering behavior of Ru atoms in UO₂ is important for achieving improved predictions of fuel evolution. First of all, it is necessary to validate that the clustering of Ru is energetically favored in UO₂ and a simple Ru dimer would be the first step of clustering. We considered three possible dimers consisting of two Ru atoms in points defect configurations (Ru_i+Ru_O, Ru_i+Ru_U, and Ru_U+Ru_O) and then found that Ru_i+Ru_U is the most energetically favored configuration among them (see Table 8). Thus we selected this configuration to assess the stability of the dimer relative to dispersed Ru atoms in UO₂. In order to do this, a separated dimer, which has a longer Ru-Ru distance (4.88 Å) than that of the bound dimer (2.51 Å), is examined (see Fig 3). The total energy of the UO₂ supercell containing the separated dimer is 0.98 eV higher than that of the bound dimer case. This

indicates that the total energy of Ru-bearing UO_2 can be lowered by the agglomeration of Ru fission products.

Table 8. Solution energies of Ru dimers in various configurations using different reference states; the lowest energies are denoted in bold.

| Dimer Configuration | Solution energy (eV) | | | | | |
|---|----------------------|---------------|--------------------|--------------------|---------------|--------------------|
| | Isolated atom | | | bulk metal | | |
| | $\text{UO}_{1.98}$ | UO_2 | $\text{UO}_{2.02}$ | $\text{UO}_{1.98}$ | UO_2 | $\text{UO}_{2.02}$ |
| $\text{Ru}_i + \text{Ru}_\text{O}$ | -6.50 | -4.01 | -1.51 | 9.10 | 11.60 | 14.10 |
| $\text{Ru}_i + \text{Ru}_\text{U}$ | -4.08 | -9.07 | -14.07 | 11.53 | 6.53 | 1.54 |
| $\text{Ru}_\text{O} + \text{Ru}_\text{U}$ | -5.14 | -7.64 | -10.14 | 10.47 | 7.97 | 5.47 |

Fig 3. The separated $\text{Ru}_i + \text{Ru}_\text{U}$ dimer (left) and the bound dimer (right) in UO_2 : Ru atoms are circled.



As presented in Fig. 3, however, a bound dimer induces large distortions in the surrounding oxygen sub-lattice (maximum displacement of matrix elements, Δd_{max} , is 0.48 Å), which possibly implies interactions between Ru and surrounding oxygen atoms, or an oxidation of the Ru atoms. This might not best represent the case in which we are interested (metallic inclusion). In addition, it is experimentally more likely that fission products reside in existing defects with free volume when they agglomerate, which are generated in a great amount during the irradiation of the fuel, rather than substitute host elements. Hence a bound Schottky defect in UO_2 is chosen as the nucleus of a nanovoid

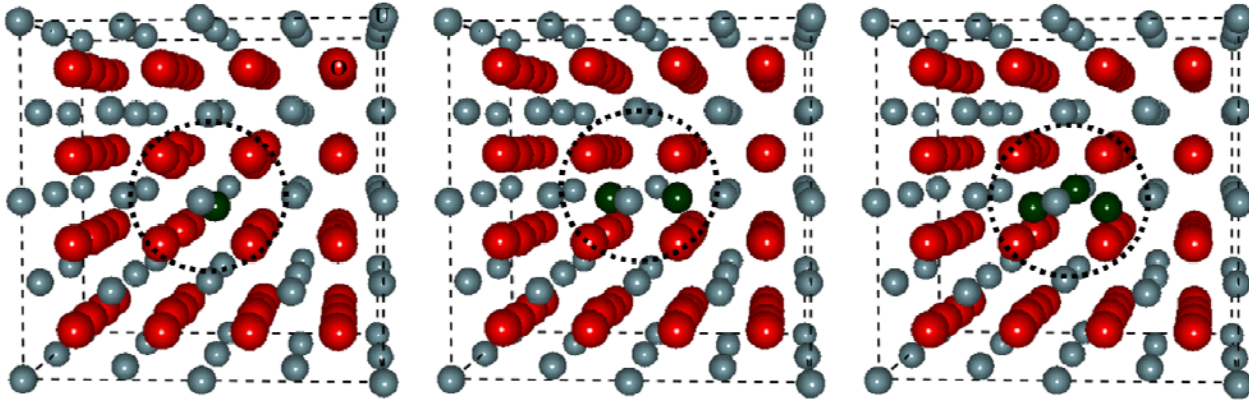
in which the fission products can easily reside. A Ru atom, dimer and trimer are then each placed in this Schottky defect and examined to understand how they evolve to a cluster. The final configurations depicted in Fig 4 indicate that even three Ru atoms are easily accommodated into the Schottky defect without significant lattice distortion ($\Delta d_{\max} = 0.14 \text{ \AA}$). This is because the Schottky defect has more free volume to contain Ru atoms than point defects (vacancies), as one would expect.

The solution and binding energies of clustered Ru are given in Table 9. The binding energy is the energy needed to bring Ru atoms in separated Schottky defects into one Schottky defect, with the remaining empty Schottky defects spaced far apart. While the binding energies indicate that it is favorable to bring two Ru atoms together into one Schottky, there is an abrupt increase in energy in going from the dimer to the trimer configuration, which implies that the dimer is the most stable Ru cluster in a Schottky defect. In fact, while dimers are bound within the Schottky, trimers are actually repelled. Therefore it is reasonable to conclude that Ru clustering occurs where there is enough empty space in the lattice, but that only a few Ru atoms can be accommodated into one Schottky, suggesting that the nucleus of the metallic inclusions may be metal dimers incorporated within Schottky defects.

Table 9. Solution and Binding energies of Ru atoms in Schottky defect in UO_2 relative to different states (a reference state of the same cluster in the vacuum (“their own reference”) or metallic Ru)

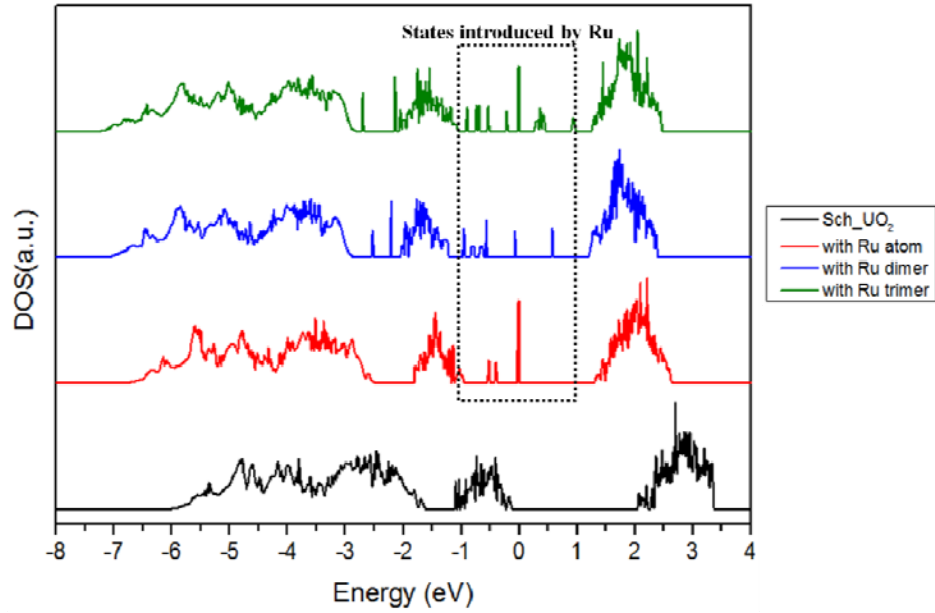
| Configuration | Solution Energy (eV) | | Binding Energy (eV) |
|---------------|----------------------|------------|---------------------|
| | their own reference | bulk metal | |
| Ru atom | -2.76 | 5.05 | - |
| Ru dimer | -2.87 | 6.86 | -0.51 |
| Ru trimer | -1.63 | 11.27 | 1.34 |

Fig 4. Ru atom, dimer, and trimer in the Schottky defect in UO_2 (circled)

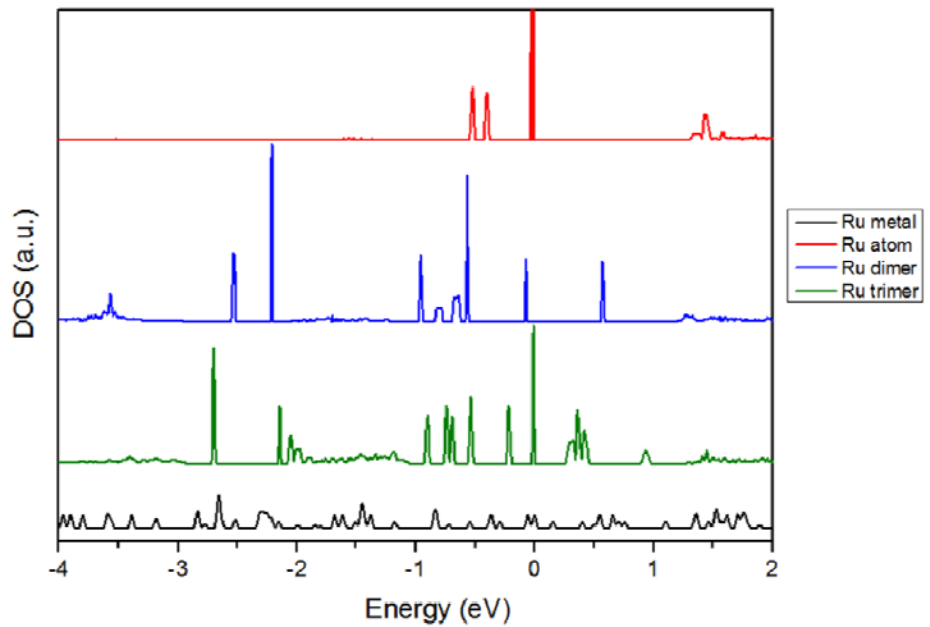


As metallic inclusions precipitate in the matrix, they will have profound effects on the fuel, modifying properties such as thermal conductivity and mechanical properties. To assess the influence of metallic aggregates on the electrical properties of the fuel, the electronic density of states (DOS) of all three cases of Ru-bearing Schottky defects are analyzed. The total DOS of Ru-bearing UO_2 shows that more electronic states are introduced within the gap of UO_2 as the Ru atoms agglomerate. Further, the partial DOS of Ru clusters confirm that even a cluster as small as the dimer or trimer shows a DOS very similar to that of metallic Ru (Fig 5). Therefore Ru clusters in UO_2 become metallic at the very earliest stage of clustering – even trimers exhibit some metallic character. This also demonstrates that current empirical potentials of FPs in UO_2 , which can only describe ionic bonding, are expected to describe even the simplest of metallic clusters poorly.

Fig 5. (a) DOS plots of the UO_2 with Ru atoms in the Schottky defect (the Fermi energies are aligned at $E=0$; that is, all states below $E=0$ are filled while those above are empty).



(b) DOS plot of the Ru metal and partial DOS plots of Ru atoms in the Schottky defect



4. Conclusions

The solubility of Ru in UO_2 and its clustering behavior have been explored using DFT. The results demonstrate that the solubility of the Ru atom is very sensitive to the reference state chosen, so a

two possible reference states are considered here. The uranium vacancy (V_U) site is found to be the most energetically favored solution site for Ru atom, which is actually soluble at V_U under hyperstoichiometric (UO_{2+x}) conditions, particularly when the reference state is bulk metal. Otherwise Ru is insoluble in UO_2 .

Further calculations for Ru dimers and trimers demonstrate that the system is stabilized when Ru atoms agglomerate together. Defect clusters in UO_2 , such as a bound Schottky, can promote Ru clustering by providing the necessary free volume in which to accommodate the Ru atoms. Binding energy calculations indicate that the size of the Ru cluster itself seems to be limited by the free volume of the defect structure where the cluster forms. In particular, the Ru dimer is the most stable cluster in the bound Schottky defect in UO_2 while the trimer is too large to be accommodated in such site. Further, the partial DOS of Ru clusters in the bound Schottky confirm that even the smallest of Ru cluster – the dimer – begins to exhibit metallic characteristics. All of these results indicate that the nucleus of the metallic inclusions in UO_2 may be the Ru dimer in a bound Schottky defect and that even small agglomerates of metallic fission products will begin to modify the electronic structures of the fuel significantly. Finally, these results suggest that the growth of metallic inclusions will occur via the diffusion and aggregation of metal-bearing Schottky defects, though such diffusion would require additional vacancies to occur.

Acknowledgement

This work was funded by DOE Nuclear Energy Fuel Cycle Research and Development (FCRD) Campaign, Nuclear Energy Advanced Modeling and Simulation (NEAMS) Program, FUELS: Integrated Performance and Safety Codes and Models project. Los Alamos National Laboratory is operated by Los

Alamos National Security, LLC, for the National Nuclear Security Administration of the US DOE under Contract No. DE-AC52-06NA25396.

References

- 1 C. R. A. Catlow, *Radiation Effects and Defects in Solids* **53**, 127 (1980).
- 2 C. R. A. Catlow, *Journal of Nuclear Materials* **79**, 432 (1979).
- 3 R. W. Grimes and C. R. A. Catlow, *Philos T Roy Soc A* **335**, 609 (1991).
- 4 W. Zhang, J. R. Smith, and X. G. Wang, *Physical Review B* **70**, 024103 (2004).
- 5 M. W. Finnis, A. Y. Lozovoi, and A. Alavi, *Annual Review of Materials Research* **35**, 167 (2005).
- 6 K. Reuter and M. Scheffler, *Physical Review B* **65**, 035406 (2001).
- 7 J. He, R. K. Behera, M. W. Finnis, X. Li, E. C. Dickey, S. R. Phillpot, and S. B. Sinnott, *Acta Materialia* **55**, 4325 (2007).
- 8 H. Y. Geng, Y. Chen, Y. Kaneta, and M. Kinoshita, *Journal of Alloys and Compounds* **457**, 465 (2008).
- 9 A. Jelea, M. Colbert, F. Ribeiro, G. Treglia, and R. J. M. Pellenq, *Journal of Nuclear Materials* **415**, 210 (2011).
- 10 T. Petit, G. Jomard, C. Lemaignan, B. Bigot, and A. Pasturel, *Journal of Nuclear Materials* **275**, 119 (1999).
- 11 H. Kleykamp, *Journal of Nuclear Materials* **131**, 221 (1985).
- 12 C. R. Stanek and R. W. Grimes, *Journal of Nuclear Materials* **282**, 265 (2000).
- 13 J. P. Crocombette, *Journal of Nuclear Materials* **305**, 29 (2002).
- 14 G. Brillant and A. Pasturel, *Physical Review B* **77** (2008).

- 15 B. Dorado, M. Freyss, and G. Martin, *Eur Phys J B* **69**, 203 (2009).
- 16 G. Brillant, F. Gupta, and A. Pasturel, *J Phys-Condens Mat* **21** (2009).
- 17 P. V. Nerikar, X. Y. Liu, B. P. Uberuaga, C. R. Stanek, S. R. Phillpot, and S. B. Sinnott, *J Phys-Condens Mat* **21** (2009).
- 18 G. Brillant, F. Gupta, and A. Pasturel, *Journal of Nuclear Materials* **412**, 170 (2011).
- 19 F. Gupta, G. Brillant, and A. Pasturel, *Philos Mag* **87**, 2561 (2007).
- 20 J. P. Crocombette, F. Jollet, L. N. Nga, and T. Petit, *Physical Review B* **6410** (2001).
- 21 M. Freyss, T. Petit, and J. P. Crocombette, *Journal of Nuclear Materials* **347**, 44 (2005).
- 22 M. Iwasawa, Y. Chen, Y. Kaneta, T. Ohnuma, H.-Y. Geng, and M. Kinoshita, *MATERIALS TRANSACTIONS* **47**, 2651 (2006).
- 23 H. Y. Geng, Y. Chen, Y. Kaneta, M. Iwasawa, T. Ohnuma, and M. Kinoshita, *Physical Review B* **77** (2008).
- 24 H. Matzke, *J Chem Soc Farad T 2* **83**, 1121 (1987).
- 25 C. G. Van de Walle and J. Neugebauer, *J Appl Phys* **95**, 3851 (2004).
- 26 P. E. Blochl, *Physical Review B* **50**, 17953 (1994).
- 27 G. Kresse and J. Hafner, *Physical Review B* **47**, 558 (1993).
- 28 G. Kresse and J. Furthmüller, *Physical Review B* **54**, 11169 (1996).
- 29 H. Wang and W. F. Schneider, *The Journal of Chemical Physics* **127**, 064706 (2007).
- 30 D. Lide, *CRC Handbook of Chemistry and Physics, 88th Edition (CRC Handbook of Chemistry & Physics)* (CRC Press, 2007).
- 31 J. P. Perdew, J. A. Chevary, S. H. Vosko, K. A. Jackson, M. R. Pederson, D. J. Singh, and C. Fiolhais, *Phys. Rev. B* **46**, 6671 (1992).
- 32 P. J. Kelly and M. S. S. Brooks, *J Chem Soc Farad T 2* **83**, 1189 (1987).

- 33 T. Petit, C. Lemaignan, F. Jollet, B. Bigot, and A. Pasturel, *Philos Mag B* **77**, 779 (1998).
- 34 V. I. Anisimov and O. Gunnarsson, *Physical Review B* **43**, 7570 (1991).
- 35 A. I. Liechtenstein, V. I. Anisimov, and J. Zaanen, *Physical Review B* **52**, R5467 (1995).
- 36 V. I. Anisimov, F. Aryasetiawan, and A. I. Lichtenstein, *J Phys-Condens Mat* **9**, 767 (1997).
- 37 L. Petit, A. Svane, Z. Szotek, and W. M. Temmerman, *Science* **301**, 498 (2003).
- 38 I. D. Prodan, G. E. Scuseria, and R. L. Martin, *Physical Review B* **76** (2007).
- 39 S. L. Dudarev, D. N. Manh, and A. P. Sutton, *Philos Mag B* **75**, 613 (1997).
- 40 B. Dorado, G. Jomard, M. Freyss, and M. Bertolus, *Physical Review B* **82** (2010).
- 41 B. Dorado, B. Amadon, M. Freyss, and M. Bertolus, *Physical Review B* **79** (2009).
- 42 H. J. Monkhorst and J. D. Pack, *Physical Review B* **13**, 5188 (1976).
- 43 P. Nerikar, T. Watanabe, J. S. Tulenko, S. R. Phillpot, and S. B. Sinnott, *Journal of Nuclear Materials* **384**, 61 (2009).
- 44 A. B. Lidiard, *Journal of Nuclear Materials* **19**, 106 (1966).
- 45 G. H. Lander, E. S. Fisher, and S. D. Bader, *Advances in Physics* **43**, 1 (1994).
- 46 C. S. Barrett, M. H. Mueller, and Hitterma.Rl, *Phys Rev* **129**, 625 (1963).
- 47 H. Zhu, C. Tang, and R. Ramprasad, *Physical Review B* **82** (2010).
- 48 J. G. Yu, R. Devanathan, and W. J. Weber, *J Phys-Condens Mat* **21** (2009).
- 49 C. Mun, L. Cantrel, and C. Madic, *Nuclear Technology* **156**, 332 (2006).
- 50 H. Y. Geng, Y. Chen, Y. Kaneta, and M. Kinoshita, *Physical Review B* **77**, 180101 (2008).
- 51 G. Busker, R. W. Grimes, and M. R. Bradford, *Journal of Nuclear Materials* **312**, 156 (2003).